Atmospheric Research 206 (2018) 1–12

Contents lists available at ScienceDirect

Atmospheric Research

journal homepage: www.elsevier.com/locate/atmosres

The effect of ice nuclei on a deep convective cloud in South China

Xin Deng, Huiwen Xue*, Zhiyong Meng

Department of Atmospheric and Oceanic Sciences, School of Physics, Peking University, Beijing, China

ARTICLE INFO

Keywords:
Ice nuclei
Deep convective cloud
Vertical transport
Ice nucleation
Homogeneous freezing
Heterogeneous nucleation

ABSTRACT

This study uses the Weather Research and Forecasting Model to simulate a deep convective cloud under a relatively polluted condition in South China. Ice nuclei (IN) aerosols near the surface are effectively transported upwards to above the 0 °C level by the strong updrafts in the convective cloud. Four cases with initial surface IN aerosol concentrations of 1, 10, 100, and 1000 L^{-1} are simulated. All simulations can well reproduce the major characteristics of the deep convective cloud in terms of the evolution, spatial distribution, and its track. IN aerosols have little effect on these macrophysical characteristics but can significantly affect ice formation. When IN concentration is increased, all heterogeneous nucleation modes are significantly enhanced, whereas the homogeneous freezing of cloud droplets is unchanged or weakened depending on the IN concentration and the development stages of the deep convective cloud. The homogeneous freezing of haze particles is generally not affected by increased IN but is slightly weakened in the extremely high IN case. As IN concentration is increased by 10 and 100 times, the enhanced heterogeneous nucleation is still not strong enough to compete with homogeneous freezing. Ice formation is hence still dominated by the homogenous freezing of cloud droplets and haze particles in the layer of 9–14 km, where most of the ice crystals are produced. The microphysical properties are generally unaffected in all the stages of cloud evolution. As IN concentration is increased by 1000 times and heterogeneous nucleation is further enhanced, the homogeneous freezing of cloud droplets and haze particles dominates only in the mature and dissipating stages, leading to unaffected ice number mixing ratio in the anvil region (approximately above 9 km) for these two stages. However, in the developing stage, when the supply of cloud droplets is limited, the homogeneous freezing of cloud droplets is weakened or even suppressed due to the very strong competition for liquid water with heterogeneous nucleation, leading to significantly lower ice number mixing ratio in the anvil regions. In addition, the microphysical properties in the convective core regions below the cloud anvil (approximately below 9 km) are also affected in the case of 1000 L^{-1}. The enhanced heterogeneous nucleation produces more ice crystals below 9 km, leading to a stronger conversion from ice crystals to snow particles, and hence higher number and mass mixing ratios of snow. The IN effect on the spatial distributions and temporal evolutions of the surface precipitation and updraft velocity is generally insignificant.

1. Introduction

Aerosols can serve as ice nuclei (IN) to facilitate ice formation at temperatures warmer than the homogeneous ice nucleation temperature (Pruppacher and Klett, 1997, p287). IN are traditionally thought to be solid, insoluble particles with crystalline structures similar to the hexagonal lattice of ice (Lamb and Verlinde, 2011, pp308). Such particles include dust, soot, and volcanic ash from either natural or anthropogenic sources (e.g., DeMott, 1990; Fornea et al., 2009). However, over the past decade, laboratory experiments showed that some organic and biological particles can also serve as IN, although without the crystalline structures similar to ice crystals (e.g., Wang et al., 2012; Hoose and Möhler, 2012; Murray et al., 2012).

Field projects such as CRYSTAL-FACE (Cirrus Regional Study of Tropical Anvils and Cirrus Layers-Florida Area Cirrus Experiment) and NAMMA (NASA African Monsoon Multidisciplinary Analyses) showed the wide existence of ice-nucleating aerosols inside ice crystals in cloud anvil of deep convective clouds. Insoluble particles (soot, organic carbon, dust, and metals) account for 51–55% on average in the number of residual nuclei collected from anvil clouds over Florida during CRYSTAL-FACE, and the ratio of insoluble to soluble (salts and sulfate) particles in small residual nuclei increases as the anvil environmental temperature increases (Twohy and Poellot, 2005). This indicates that insoluble particles play an important role in triggering ice formation at warmer temperatures in cirrus anvil. Twohy (2015) found that dust is the dominant residual particle type sampled in ice crystals

* Corresponding author at: Department of Atmospheric and Oceanic Sciences, School of Physics, Peking University, Room 518 North, Physics Building, 209 Chengfu Road, Beijing 100871, China.
E-mail address: hxue@pku.edu.cn (H. Xue).

https://doi.org/10.1016/j.atmosres.2018.02.013
Received 18 November 2017; Received in revised form 15 February 2018; Accepted 15 February 2018
Available online 17 February 2018

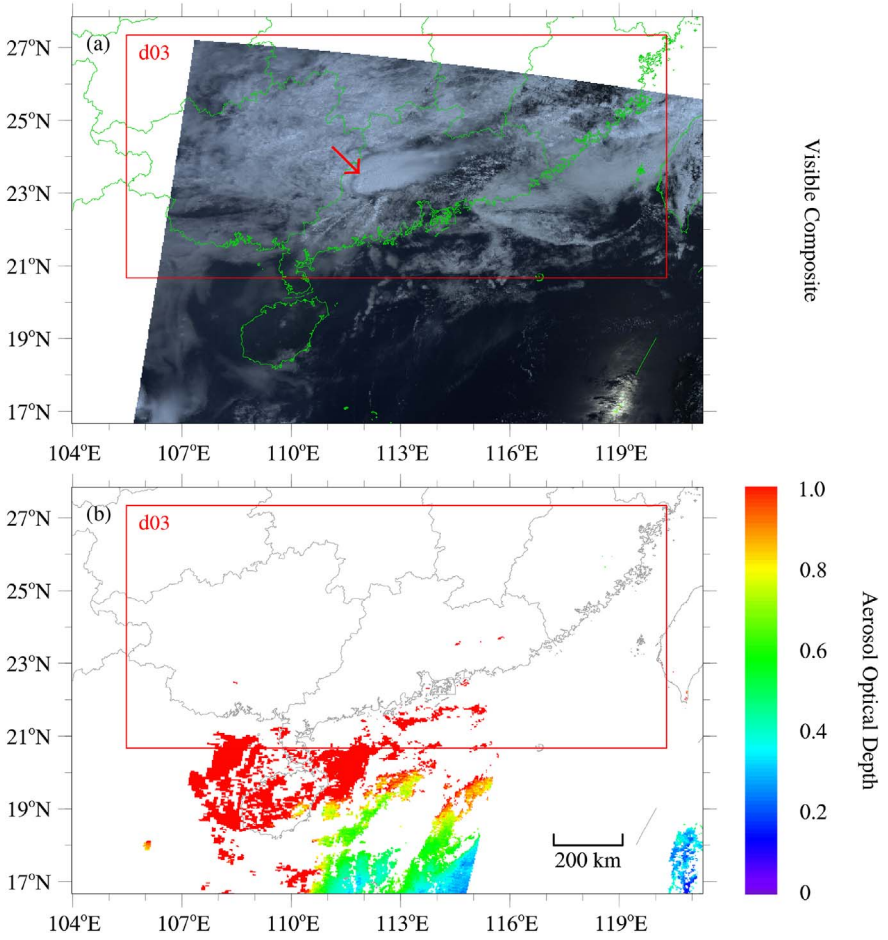

Fig. 1. MODIS images of (a) visible composite and, (b) aerosol optical depth at local time 10:50 on 17 April 2011. The red boxes indicate the location of innermost domain (d03). The red arrow in (a) indicates the location of the deep convective cloud. (For interpretation of the references to color in this figure legend, the reader is referred to the web version of this article.)

from anvil outflow of tropical Eastern Atlantic Ocean during NAMMA, which is downwind of the Saharan dust source.

Results from some numerical simulations indicate that increasing IN concentration can increase cloud ice amount in deep convective clouds. For example, van den Heever et al. (2006) showed that high IN concentration in the dust layer leads to higher proportion of vertically integrated ice water in the total condensate (liquid and ice) in a CRYSTAL-FACE case using the Regional Atmospheric Modeling System (RAMS). Similar results were also found in a large eddy simulation (LES) (Carrió et al., 2007). Fan et al. (2010) employed a 3-dimensional cloud resolving model to simulate the IN effect on two deep convective clouds over Tiwi Islands, northern Australia. They found that both ice number concentration and ice water content increase dramatically when multiplying the IN concentration by a factor of 2.5 either in the mid-troposphere only or in the whole vertical extent of the troposphere.

Increasing IN concentration can sometimes decrease the ice water content. In a LES study of the IN effect on a deep convective cloud over Tiwi Islands (Connolly et al., 2006), the number concentration of the total ice particles (ice, snow and graupel) increases when enhancing heterogeneous ice nucleation by five times, but decreases when enhancing by ten times. However, in a Weather Research and Forecasting (WRF) model simulation of a deep convective cloud over tropical western Pacific (Phillips et al., 2007), it was found that the cloud is hardly affected when IN concentration is increased by 10 times but significantly affected when IN concentration is increased by 1000 times. In the extremely high IN case, ice concentration is increased by up to half an order of magnitude at lower altitude (below −20 °C level) due to the enhanced heterogeneous nucleation, while reduced by up to one order of magnitude at higher altitude because homogeneous freezing of cloud droplets is suppressed by the decreased liquid water.

The IN impact on the updrafts and precipitation of deep convections is largely uncertain, with regard to both the magnitude and the sign. Some studies suggested that more IN result in more latent heat release during glaciation and therefore stronger updrafts. More ice particles can also produce more precipitation through stronger depositional growth and collection of cloud droplets (Ekman et al., 2007; Hazra et al., 2016). But van den Heever et al. (2006) demonstrated a decrease of the 12-h accumulated precipitation with increasing IN, although the precipitation in the initial stage (first 6 h) increases with IN concentration. Some investigations argued that the effect of IN on the strength and surface precipitation of deep convections are limited (Connolly et al., 2006; Fan et al., 2010). The reason is that cloud ice is not enough and mainly exists at high altitudes, thus the latent heat released by the increased ice mass mainly heats the upper level and is less important than other microphysical processes (Fan et al., 2010).

IN can nucleate ice crystals via four ice nucleation modes: deposition nucleation, condensation freezing, contact freezing, and immersion freezing (Lamb and Verlinde, 2011, pp312). Sensitivity experiments with RAMS showed that deposition-nucleation/condensation-freezing is an important mechanism of ice formation only when temperature is colder than −10 °C, while contact freezing is efficient only when temperature is warmer than −15 °C (Cotton et al., 1986). Hiron and Flossmann (2015) used a 1.5-dimensional dynamic framework coupled with bin-resolved microphysics to study the role of different ice nucleation modes in convective clouds. They found that homogenous freezing and immersion freezing dominate ice formation in convective clouds. Condensation freezing also plays an important role. On the contrary, deposition nucleation and contact freezing are much less

efficient and hence have a negligible effect on convective clouds. For the purpose of simplification, most previous simulations of real cases considered some modes of heterogeneous nucleation while neglected the others. As a result, the effect of IN may be underestimated, and the relative importance of each ice nucleation mode is therefore unclear. The fact that different studies considered different ice nucleation modes or used different ice nucleation parameterizations even for the same mode might also contribute to the big uncertainty of the IN effect in previous studies.

The purpose of this study is to investigate the effect of IN on a deep convective cloud, as well as the vertical transport of aerosol by the deep convective cloud. Section 2 introduces the case and the model used in this study. Section 3 presents the comparison between observations and model simulations, and the vertical transport of aerosol by the deep convective cloud. Section 3 also presents the contribution of different heterogeneous ice nucleation modes and the effect of IN number concentration on the microphysical and macrophysical properties of the deep convective cloud. Sections 4 and 5 respectively describe the discussions and the conclusion.

2. Case and model

2.1. The deep convective cloud case

A deep convective cloud occurring on 17 April 2011 in South China is selected for this study. The deep convective cloud was triggered in the early morning. It became stronger as it moved to the southeast, and weakened in the evening over the ocean. Fig. 1 shows the MODIS (Moderate Resolution Imaging Spectroradiometer) visible composite and aerosol optical depth (AOD) at local time 10:50 on 17 April 2011 in the region. The deep convective cloud, with a cloud top temperature as low as about −78 °C, is indicated by a red arrow in Fig. 1a.

The AOD data over the cloud-free regions indicate that AOD is very high (close to one and even higher than one) in the coastal region, and decreases from the coastline to the ocean (Fig. 1b). We therefore assume that the aerosol loading is relatively high at that time over the land in South China, where the deep convective cloud formed and developed. The high AOD in this area indicates a high concentration of cloud condensation nuclei (CCN) aerosols. If the pollution aerosols are mainly soluble particles or particles coated with soluble species, the ice nucleating ability of these particles will be relative low and hence the concentration of IN aerosols will be relatively low. Oppositely, if the pollution aerosols consist of some species with relatively high ice nucleating efficiency, there will be a possibility that the concentration of IN aerosols is relatively high. For example, many anthropogenic aerosols in the polluted cases such as soot and dust emitted by burning and mining are common types of IN. Murray et al. (2012) estimated that the potential IN concentration of soot and mineral dust can be up to 100 cm^{-3} at temperatures between −12 to −35 °C. Therefore, we can use a wide range of IN concentration in this study to represent all possible conditions.

2.2. General description of the model

In this study, we use the WRF Model version 3.6.1, which is widely used in both atmospheric research and operational prediction. The model physics includes the Yonsei University (YSU) planetary boundary layer (PBL) scheme (Hong et al., 2006), the unified Noah land surface model (Chen and Dudhia, 2001), the Rapid Radiative Transfer Model (RRTM) shortwave radiation (Mlawer et al., 1997), the New Goddard longwave radiation (Chou and Suarez, 1999), and Grell-Freitas cumulus scheme (Grell and Freitas, 2013). The NSSL two-moment bulk microphysics scheme (e.g., Mansell et al., 2010) is employed to simulate the microphysical processes of five hydrometeors (cloud droplet, rain, cloud ice, snow, and graupel).

Two types of aerosols are considered in the NSSL microphysics scheme in this study. One type can act as CCN and the other type can act as IN. Once an aerosol particle becomes active and converts into a droplet or ice crystal, it is eliminated from the total aerosols. However, other sources and sinks of aerosol, such as surface emission, secondary formation, sub-scale entrainment near the cloud base and edges, as well as aerosol dry deposition and washout (aerosol scavenging through collection by falling hydrometeors), are not considered.

The parameterization of cloud droplet formation process at the cloud base follows $N_{CCN} = CS^k$ (Twomey, 1959), where C is the number concentration of active CCN at 1% supersaturation, k is the CCN activity property of aerosol, and S is the supersaturation that can be diagnosed with the vertical velocity velocity as described in Mansell et al. (2010). Cloud droplets can also be activated within the cloud, depending on the gradient of supersaturation S. The parameter C is the prognostic variable in this study and is used to describe the CCN amount.

The parameterizations of ice formation are described in Section 2.3. The total number centration of IN aerosols is predicted in this study. We assume that all IN aerosols have exactly the same properties, and can take effect through any of the heterogeneous nucleation modes considered in this study. Therefore, the ice formation through contact freezing, deposition-nucleation/condensation-freezing, and immersion freezing in every grids and at each time step are all calculated with the total IN aerosol concentration.

There are three nested domains with horizontal sizes of 3807 × 2430, 2349 × 1458, and 1461 × 720 km^2, and horizontal resolutions of 27, 9, and 3 km, respectively. The model top extends to 50 hPa, with 12 layers below 2.5 km and 28 layers above 2.5 km. The innermost domain d03 covers the track of the convective cloud and is shown with the red boxes in Fig. 1. All the analyses in this study focus on the d03 domain only. Cumulus parameterization is turned off in d03. Therefore, precipitation in d03 is predicted by the microphysics scheme only. Precipitation in the outer two domains is predicted by both the microphysics scheme and cumulus parameterization. The initial and boundary conditions of the meteorological field are based on the 1° × 1° 6-h NCEP (National Centers for Environmental Prediction) reanalysis data. The simulations begin at local time 20:00 on 16 April 2011, with the first 6 h used as spin-up time and the next 24 h (2:00 17 April to 2:00 18 April) used for analysis. Three snapshots, 8:00, 14:00, and 20:00 on 17 April, are chosen to represent the developing, mature, and dissipating stages of the deep convective cloud, respectively.

2.3. Parameterization of ice nucleation

In the original version of the NSSL scheme, heterogeneous ice nucleations through contact freezing, deposition nucleation, and condensation freezing are considered. The parameterization of contact freezing in the NSSL scheme is described in Walko et al. (1995), where ice formation rate depends on the concentrations of active contact freezing IN and cloud droplets, the average droplet size, as well as the efficiency factor due to Brownian motion, thermophoresis, and diffusiophoresis. The concentration of active contact freezing IN is diagnosed from temperature only, and does not reflect the large variability of aerosol concentration in the atmosphere. Deposition nucleation and condensation freezing are parameterized together in the NSSL scheme because it is difficult to distinguish deposition nucleation and condensation freezing during measurements. The parameterization of deposition-nucleation/condensation-freezing in the origin NSSL scheme is based on Phillips et al. (2007), where empirical relationships between ice number concentration and supersaturation are used for two temperature ranges. For the temperature range of −5 °C to −30 °C, the empirical relationship is from the surface measurements in Meyers et al. (1992), but rescaled with a normalization factor for use in the free troposphere where IN is less rich; for temperature below −30 °C, the empirical relationship is based on the measurement in cirrus clouds in DeMott et al. (2003a).

The parameterizations of contact freezing, deposition nucleation,

and condensation freezing in the original version of the NSSL scheme are based on measurements in relatively clean conditions, with the measured IN concentration ranging from 0.1 to 10 L^{-1}. In order to investigate the IN effect in polluted conditions (e.g., for the case in this study), we revise the parameterizations of ice formation by multiplying a factor to represent the amount of IN aerosols. The factor is the ratio of the predicted concentration of IN aerosols at each grid point and at each time step to a reference IN aerosol concentration (assumed to be 1 L^{-1} in our study, within the range of the measured IN concentration that is used in the original parameterization in NSSL). It is not a constant, but varies with grid points and time.

Immersion freezing is not considered in the original NSSL scheme. We introduce the parameterization of immersion freezing into the model in this study. The ice formation rate through immersion freezing depends on surface nucleation rate (nucleation events on IN per unit surface area per unit time), IN surface area per droplet, as well as the number concentration of droplets containing immersion IN. Based on laboratory experiments of kaolinite particles with various sizes, Murray et al. (2011) proposed a temperature-dependent parameterization to predict surface nucleation rate. The data of Murray et al. (2011) was validated in the intercomparison of laboratory experiments in Hoose and Möhler (2012). The parameterization has also been used in model studies (e.g., Hiron and Flossmann, 2015). It is assumed that one droplet contains only one IN with a surface area of 1.18×10^{-13} m^2, which is the mean value in the measurements of Murray et al. (2011) and is equivalent to a radius of 0.097 μm for a spherical kaolinite particle. Considering that the number of IN particles is generally several orders of magnitude lower than liquid droplets, the number concentration of droplets containing immersion IN is assumed equal to the number concentration of immersion IN.

Primary ice crystals are produced not only by heterogeneous nucleation, but also by homogeneous freezing. In the original version of the NSSL scheme, homogeneous freezing of cloud droplets is predicted based on Bigg (1953), which calculates the fraction of frozen droplets as a function of temperature and drop diameter. For this study, we replace it with the classical ice nucleation theory. The homogeneous nucleation rate (nucleation events in droplets per unit volume per unit time) is parameterized as in Murray et al. (2011). The homogenous freezing of haze particles is not considered in the original version of NSSL, and we introduce it into the WRF model following DeMott et al. (1994). The parameterization of homogenous freezing of haze particles depends on the temperature and supersaturation with respect to water, as well as the predicted number concentration of CCN aerosols. The homogenous freezing of haze particles is calculated only at temperatures colder than −35 °C.

In addition to primary ice nucleation, secondary ice production is also considered in our model. The fragmentation of crystals, the fragmentation of relatively large cloud droplets during freezing, and splintering process during the riming growth of large graupel are the most important secondary ice production mechanisms in literatures (Pruppacher and Klett, 1997, p355–360). These three processes are all considered in this study. The parameterization of crystal fragmentation only involves the relatively large snow particles, which is based on Schuur and Rutledge (2000). The fragmentation of relatively large cloud droplets is calculated when the super-cooled liquid droplets freeze through homogenous freezing or contacting with ice crystals. The observed ice particle enhancement factor (defined by Mossop, 1970 as the ratio of ice particles produced to drops frozen) generally ranges between 1 and 2 (Pruppacher and Klett, 1997, pp357), and is assumed as 1 in our model. The ice splintering during the riming growth of large graupel is known as the Hallett-Mossop process (e.g., Hallett and Mossop, 1974; Mossop and Hallett, 1974), and is parameterized following Ziegler et al. (1986).

2.4. Aerosol set up

The initial profiles for the CCN and IN aerosols are prescribed for the whole domain. Below 850 hPa, the aerosols are well mixed so that the number mixing ratios of both types of aerosols are constant. Above 850 hPa, the aerosol number concentrations decrease exponentially with height with a scale height of 3 km (e.g., Léon et al., 2009; Yu et al., 2010). The profiles for both types of aerosols at the boundaries of the three domains for the whole simulation time are set to be the same as the initial profiles.

Initially, the parameter C (for describing CCN amount) is set as 1.5×10^4 cm^{-3} near the surface, as derived from the observation in the relatively polluted area in China (e.g., Rose et al., 2010; Deng et al., 2013). The parameter k (for describing the CCN activity property) is fixed at 0.65 throughout the simulation time, based on the CCN measurement in China (e.g., Deng et al., 2013). All simulations are initialized with the same C and k because we do not study the CCN effect but focus on the IN effect only.

Four experiments are performed with different concentrations of IN aerosols. In the low IN case, which represents a clean condition, the initial IN aerosol number concentration is 1 L^{-1} near the surface; in the intermediate and high IN cases, which represents the relatively polluted conditions, the initial IN aerosol number concentration is 10 and 100 L^{-1} near the surface. The number concentrations of IN aerosols in the three cases are all within the range of observations (< 0.1–500 L^{-1}) (e.g., Rogers et al., 1998; Yin et al., 2012; Jiang et al., 2014). We also investigate an extremely high IN case (1000 L^{-1}) for a sensitivity study. Such a high IN concentration is close to the recorded extremely high IN conditions, such as dust events or severe pollution (10^2– $> 10^3$ L^{-1}) (e.g., DeMott et al., 2003b; Yin et al., 2012; Jiang et al., 2016).

3. Results

3.1. Comparison between observations and simulations

Fig. 2 shows the observed radar reflectivity (left column) and the simulated radar reflectivity in the low IN case (right column) at various stages. At 8:00, the deep convective cloud is in the developing stage, and has already produced heavy precipitation (with high radar reflectivity) in some regions (Fig. 2a). Then the deep convective cloud moved to the southeast and produced heavy precipitation in larger areas near the coast of South China at 14:00 (Fig. 2c). When the deep convective cloud moved further southeast over the ocean at about 20:00, precipitation covered an even larger area but was not so strong as that at 14:00 (Fig. 2e). The simulation well reproduces the major characteristics of the deep convective cloud in terms of the evolution, spatial distribution, and track of the observed radar reflectivity overall, although the simulated radar reflectivity is generally higher than the observation throughout the evolution of the deep convective cloud. The simulation also misses out the stratiform clouds and its precipitation at the northeast corner of d03 in the morning (as shown in Fig. 2a). The stratiform clouds are not directly associated with the deep convective cloud that we focus on in this investigation and thus are not included in the analysis here.

The other cases with higher IN concentration show similar evolution and distribution of base radar reflectivity. The location of heavy precipitation, especially in the mature stage, and the moving track of the deep convective cloud is also similar in all cases. The approximate track of the deep convective cloud is shown as a straight line in Fig. 2, which is used for the discussion in Section 3.2.

3.2. Vertical transport of IN aerosols by the deep convective cloud

The left column in Fig. 3 shows the vertical cross sections of the IN aerosol number mixing ratio along the approximate track of the deep convective cloud at various stages for the low IN case. Contours of the

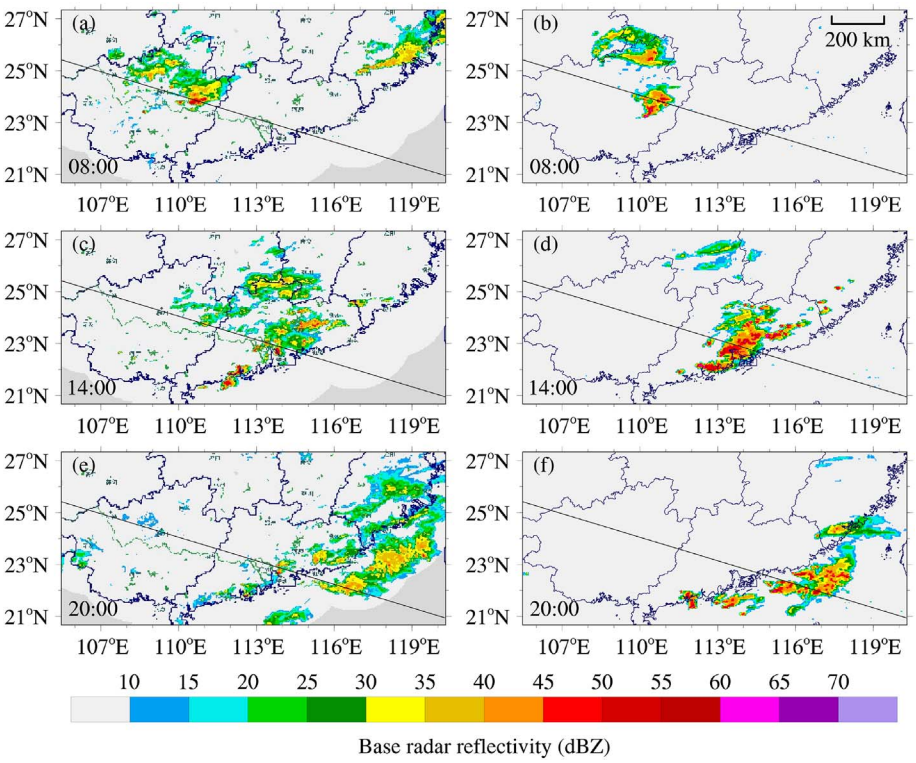

Fig. 2. The observed (left column) and low IN case simulated (right column) base radar reflectivity of the deep convective cloud at local time (a–b) 8:00, (c–d) 14:00, and (e–f) 20:00. The black lines are the approximate track of the deep convective cloud.

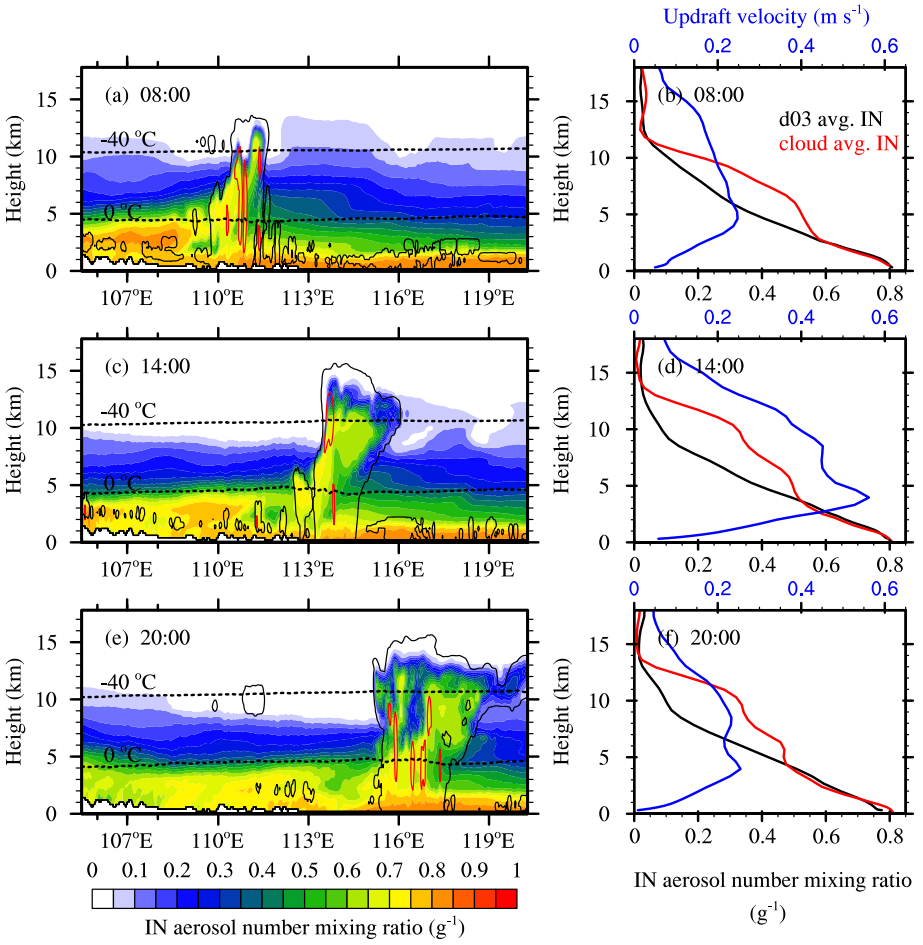

Fig. 3. The vertical cross sections (left column) and averaged vertical profiles (right column) of the IN aerosol number mixing ratio along the track of the deep convective cloud (the black lines in Fig. 2) at local time (a and b) 8:00, (c and d) 14:00, and (e and f) 20:00. The black curves in the left column indicate the regions with total hydrometeors mixing ratio > 0.01 g kg^{-1} and the red curves indicate updrafts with vertical velocity > 1 m s^{-1}. The dot lines in the left column show the heights of 0 and −40 °C. The black lines in the right column represent the d03 domain-averaged number mixing ratios of IN aerosols, and the red lines represent the cloud-averaged (averaged over the cloudy columns, similarly hereinafter) number mixing ratios of IN aerosols. The blue lines represent the cloud-averaged updraft velocity (averaged over the grid points with positive velocity in the cloudy columns). (For interpretation of the references to color in this figure legend, the reader is referred to the web version of this article.)

total mass mixing ratio of all hydrometeors and updrafts are also shown in the left column of Fig. 3 to indicate the structure of the deep convective cloud. The right column in Fig. 3 presents the corresponding vertical profiles of the domain-averaged and cloud-averaged (averaged over the cloudy columns of the deep convective cloud) IN aerosol number mixing ratios, as well as the cloud-averaged updraft velocity (averaged over all grid points with positive vertical velocity in the cloudy columns) are also shown. We only show the low IN case as an example to discuss the vertical transport of IN aerosols. The other cases have similar spatial distribution of IN aerosols except that the overall IN aerosol number mixing ratio is higher. The vertical profiles of cloud-averaged updraft velocity are also similar in all cases. The cloud top height is about 14.6 km (~ −71 °C) at 8:00, increases to 16.5 km (~ −80 °C) in the mature stage at 14:00, and then decreases to 15.8 km (~ −79 °C) at 20:00. The simulated cloud top temperature at 11:00 is about −77 °C, and agrees well with the observed −78 °C from MODIS at 10:50. The 0 °C level for this convective cloud locates at about 4 km, and the −40 °C level locates at about 10 km.

The deep convective cloud is in the developing stage when arriving in the region around 111°E at local time 8:00 (Fig. 3a). The IN aerosol profile in Fig. 3b indicates that the IN aerosol number mixing ratio near the surface is about 0.8 g^{-1} (equivalent to a number concentration of 0.98 L^{-1} with the standard air density of 1.225 kg m^{-3}), which is close to the initial number concentration of 1 L^{-1}. The IN aerosol number mixing ratio inside the convective cloud can be as high as 0.8 g^{-1} at 4 km, and still as high as 0.7 g^{-1} at 10 km. The maximum updraft velocity is 11.5 m s^{-1} (figure not shown). The cloud-averaged updraft velocity peaks at about 5 km with a value of 0.25 m s^{-1}. With the help of the strong updrafts in the deep convective cloud, IN aerosols are transported upwards to the upper troposphere very efficiently. The cloud-averaged IN aerosol number mixing ratio is hence significantly higher than the d03 domain-averaged between 3 and 11 km. After IN aerosols are transported to the upper troposphere, they can take effect and produce ice crystals through heterogeneous nucleation. In the regions east of the deep convective cloud, most IN aerosols are limited in the boundary layer, because it is difficult for the air mass near the surface to break through the boundary layer without strong updrafts.

The deep convective cloud keeps developing and the cloud top reaches about 16 km, with cloud anvils extending to larger areas at 14:00 and 20:00 (Fig. 3c and e). The maximum updraft velocity increases to 25.5 m s^{-1} at 14:00 and 18.4 m s^{-1} at 20:00 (figures not shown). At 14:00, the cloud-averaged updraft velocity peaks at about 4 km with a value of 0.56 m s^{-1}, and is still as high as 0.25 m s^{-1} at 13 km. The significantly stronger updrafts at the mature stage transport the IN aerosols to altitudes even higher than in the developing stage. In the mature and dissipating stages, the maximum number mixing ratio of IN aerosol remains as 0.7 g^{-1} at 10 km. IN aerosols can have a number mixing ratio of 0.5 g^{-1} in the cloud anvil region. It is also seen that the surface number mixing ratio of IN aerosols in the regions west of the deep convective cloud is lower compared to the regions east of the convection where vertical transport has not occurred. The high IN aerosol number mixing ratio in the convective core regions and the anvil regions indicates the importance of applying the number concentration of IN aerosols to the parameterizations of heterogeneous ice formation rate in deep convective cloud. As shown in Fig. 3d and f, the difference between the cloud-averaged and d03 domain-averaged IN aerosol number mixing ratios becomes much more obvious at 14:00 and 20:00 than at 8:00, especially above 10 km. The cloud-averaged IN aerosol number mixing ratio near 10 km is almost four times of the d03 domain-averaged.

3.3. The contribution of different ice nucleation modes to ice formation

Fig. 4 shows the cloud-averaged ice formation rates (the number of nucleated ice crystals per unit mass of air per unit time) through contact freezing (CF), deposition-nucleation/condensation-freezing (DCF), immersion freezing (IF), and homogeneous freezing of cloud droplets and haze particles (HOMO) at local time 8:00 (developing stage), 14:00 (mature stage) and 20:00 (dissipating stage) for the low and high IN cases. It is seen that different ice nucleation modes prefer to occur at different temperature ranges and hence dominate at different heights. Increasing IN concentration by 10, 100, and 1000 times does not change the peak height but significantly increase the magnitude of ice formation rates for all the heterogeneous nucleation modes at all

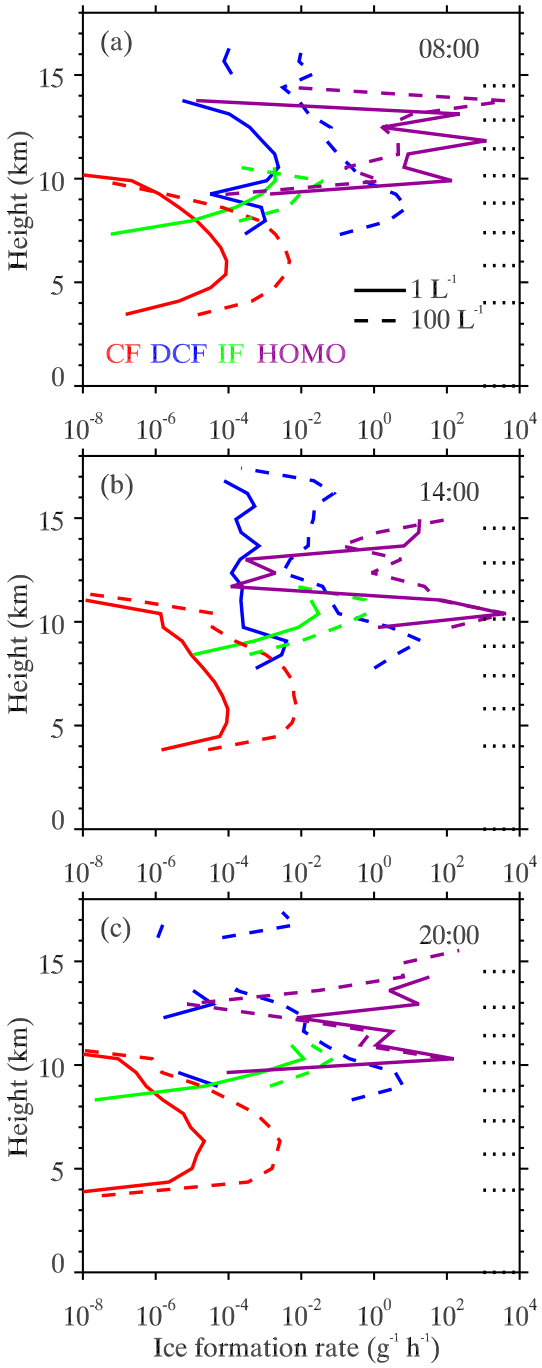

Fig. 4. The cloud-averaged vertical profiles of ice formation rates through contact freezing (red lines), deposition-nucleation/condensation-freezing (blue lines), immersion freezing (green lines), and homogeneous freezing of cloud droplets and haze particles (purple lines) at local time (a) 8:00, (b) 14:00, and (c) 20:00. The solid lines are for the low IN case, and the dashed lines are for the high IN case. Dotted lines near the right y-axis indicate the heights with d03 domain-averaged environment temperature at 0, −10, −20, −30, −40, −50, −60 and −70 °C. (For interpretation of the references to color in this figure legend, the reader is referred to the web version of this article.)

heights.

Contact freezing mainly occurs between 4 and 11 km (about 0 to −45 °C). The ice formation rate due to contact freezing peaks at 6–7 km, where the temperature is between −10 and −20 °C. Below 6 km, the rate of ice formation through contact freezing increases with height because the concentration of active IN increases with decreasing temperature. Above 7 km, the rate of ice formation through contact freezing decreases with height because the active IN concentration is limited by the relatively low aerosol concentration, and more importantly, because the lower temperature reduces the Brownian motion of aerosol particles and hence the probability of aerosol contacting with liquid droplets. Contact freezing is the only nucleation mode that is active below 7 km.

Deposition-nucleation/condensation-freezing mainly occurs between 7 and 17 km, where the temperature ranges from −20 °C to −80 °C. Deposition-nucleation/condensation-freezing are the only heterogeneous nucleation modes that can occur above 11 km (−45 °C), where nearly no cloud droplets exist and hence contact freezing, immersion freezing, as well as homogenous freezing of cloud droplets, are all suppressed.

Immersion freezing mainly occurs from 7 to 11 km (−20 to −45 °C), while homogeneous freezing of cloud droplets and haze particles mainly occurs at the layer between 9 and 14 km (−30 to −75 °C), indicating that immersion freezing starts to take effect at lower altitudes (warmer temperature) than homogeneous freezing. The homogenous freezing of cloud droplets mainly occurs from 9 to 11 km (−30 to −45 °C), while from 11 to 14 km (−45 to −75 °C), there is nearly no homogenous freezing of cloud droplets due to the lack of liquid water. Oppositely, the homogenous freezing of haze particles can occur without any liquid water, but generally requires colder temperature. Therefore, the homogeneous freezing of haze particles mainly occurs in the layer of 11 to 14 km. The ice formation rates through immersion freezing and homogeneous freezing of cloud droplets have similar vertical variation, with the peak of ice formation rate at about 10 km, where the temperature is −40 °C approximately. Below 10 km, they both increase with altitude because of the decreasing temperature. Above 10 km, they both decrease with altitude because of the decreasing amount of cloud droplets.

In the low IN case (1 L^{-1}), each layer has a dominant ice nucleation mode and the dominant mode does not change as the convection evolves. Ice formation is dominated by contact freezing below 7 km, and by deposition-nucleation/condensation-freezing at 7–9 km. In the layer of 9–11 km, immersion freezing is the most efficient heterogeneous nucleation mode but its nucleation rate is still several orders of magnitude smaller than that of homogeneous freezing. Homogeneous freezing is the dominant nucleation mode not only in the layer of 9 to 11 km, which mainly owes to the homogeneous freezing of cloud droplets, but also in the layer of 11 to 14 km, which mainly owes to the homogeneous freezing of haze particles. Above 14 km, ice formation is totally dominated by deposition-nucleation/condensation-freezing. Note that in addition to heterogeneous nucleation, the secondary ice production can also occur in the layer of 4–9 km (0 to −30 °C) with a peak at about 5 km, and hence can also considerately contribute to the formation of ice crystals at low altitudes.

When IN concentration is increased by 10 times (figure not shown), the ice formation rate in all heterogeneous nucleation modes are increased by about one order of magnitude. Therefore, for the layers below 7 km, 7–9 km, and above 14 km, the overall ice formation rate is one order of magnitude higher. However, for the layer of 9–14 km, where most of the ice crystals are produced, the ice formation rates through homogeneous freezing of cloud droplets and haze particles are almost unaffected, and therefore the overall ice formation rate is similar to the low IN case. The dominant ice nucleation mode in each layer is the same as in the low IN case, and does not change as the deep convective cloud evolves.

When IN concentration is increased by 100 times (dashed lines in Fig. 4), the ice formation rates in all heterogeneous nucleation modes are increased by about two orders of magnitude and heterogeneous nucleation becomes more competitive with the homogeneous freezing of cloud droplets. For the layers below 7 km, 7–9 km, and above 14 km, the overall ice formation rate is significantly higher compared to the low IN case. The enhanced heterogeneous ice nucleation leads to enhanced growth of ice crystals and depletion of cloud droplets. Therefore, the homogeneous freezing from 9 to 14 km may also be affected. In the developing stage, when the amount of cloud droplets is not very high in the relatively weak updrafts, the ice formation rate through homogenous freezing of cloud droplets decreases by two orders of magnitude at the peak (about 10 km) as the IN concentration is increased by 100 times. Therefore, for the 9–11 km layer, the enhanced deposition-nucleation/condensation-freezing becomes comparable with the weakened homogenous freezing of cloud droplets, and the overall ice formation rate is decreased with the increased IN concentration by 100 times. However, for the 11–14 km layer, where the ice formation rate is even higher than the 9–11 km layer, increasing IN concentration by 100 times results in almost unaffected homogeneous freezing of haze particles and hence almost unchanged overall ice formation rate. In the mature and dissipating stages, when the cloud droplet supply is abundant, the ice formation rate due to homogenous freezing of cloud droplets is almost the same as that in the low and intermediate IN cases. The homogenous freezing of haze particles is still almost unaffected by IN. The overall ice formation rate in the layer of 9–14 km hence is almost unaffected by IN aerosols in the mature and dissipating stages.

When the IN concentration is further increased to be extremely high (1000 L^{-1}), the ice formation rates of all the heterogeneous modes, especially the deposition-nucleation/condensation-freezing mode, are increased even further, so that the ice formation rate in the layers below 7 km, 7–9 km, and above 14 km are all increased by more than two orders of magnitude (figure not shown). For the layer of 9–11 km, the homogeneous freezing of cloud droplets is completely suppressed in the developing stage, and therefore the significantly enhanced deposition-nucleation/condensation-freezing become the dominant nucleation modes at that time. For the layer of 11–14 km, the homogeneous freezing of haze particles is also slightly weakened, but is still the dominant nucleation mode. Therefore the overall ice formation rate is decreased from 9 to 14 km. In the mature and dissipating stages, however, homogenous freezing of cloud droplets and haze particles, as well as the overall ice formation rate, are almost not affected even if the IN concentration is increased by 1000 times.

3.4. The IN effect on the microphysical properties of the deep convective cloud

In all the simulated cases, the number and mass mixing ratios of all hydrometeors, generally increase as the deep convective cloud evolves from the developing stage to the mature stage, and then decrease as the cloud evolves into the dissipating stage. Overall, increasing IN concentration by 10 and 100 times has nearly no influence on the number and mass mixing ratios of hydrometeors, except that the graupel number mixing ratio in the convective core regions (approximately below 9 km) becomes higher. Increasing IN concentration by 1000 times can lead to some obvious changes, especially the snow mass and number mixing ratios in the convective core regions and the ice number mixing ratio in the anvil regions (approximately above 9 km).

The vertical profiles of the cloud-averaged number and mass mixing ratios of all hydrometeors for the low IN case (1 L^{-1}) and high IN case (100 L^{-1}) are presented in Fig. 5. Ice crystals are mainly in the layer of 11–14 km. The ice number mixing ratios in the low IN and high IN cases are not significantly different throughout the evolution of the deep convective cloud. This is because the overall ice formation rate in the high IN case is similar to that in the low IN case for the layer of 11–14 km, where most of the ice crystals are produced and are mainly produced through the homogeneous freezing of haze particles (see

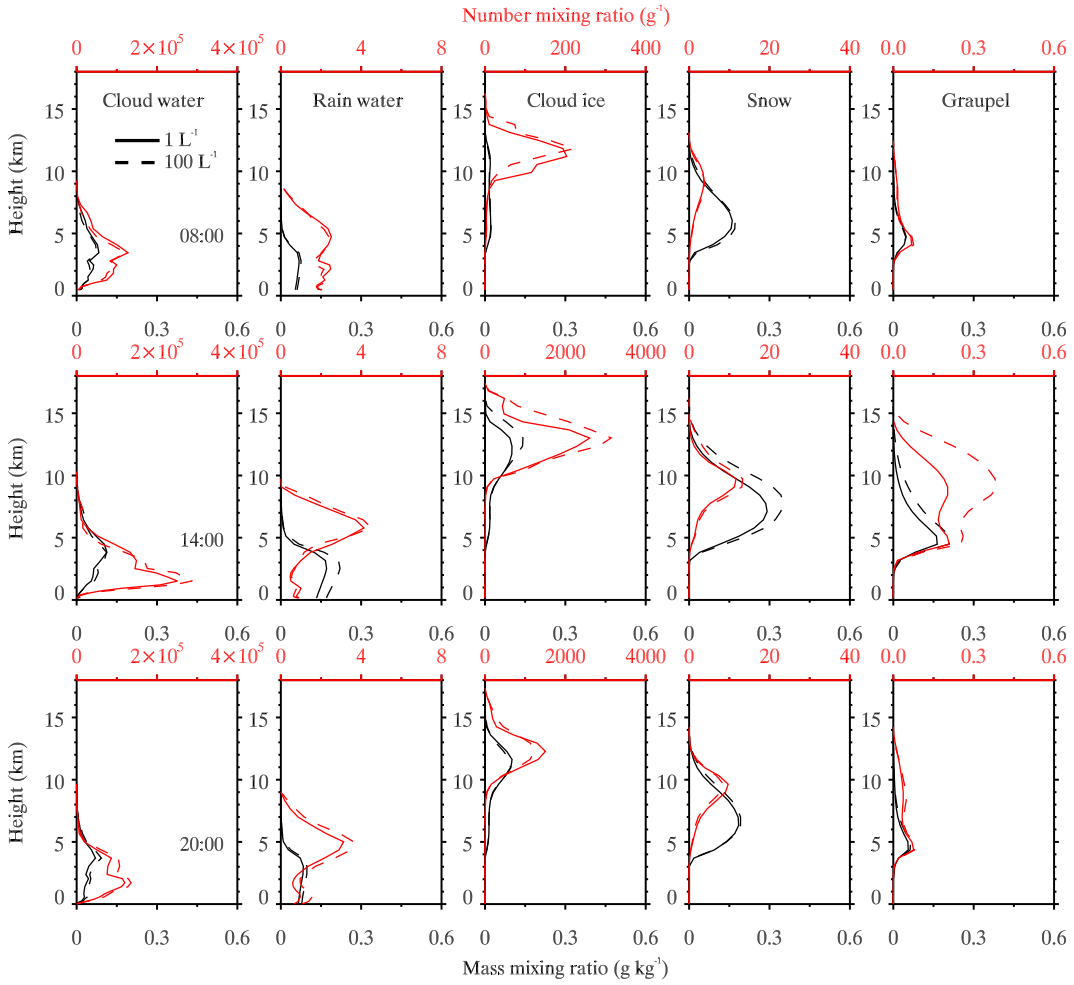

Fig. 5. The cloud-averaged vertical profiles of the mass mixing ratios (black lines) and number mixing ratios (red lines) of all hydrometeors at local time 8:00 (upper row), 14:00 (middle row), and 20:00 (bottom row). Hydrometeors include cloud water (first column), rain water (second column), cloud ice (third column), snow (fourth column) and graupel (fifth column). Solid lines are for the low IN case (1 L^{-1}), and the dashed lines are for the high IN case (100 L^{-1}). (For interpretation of the references to color in this figure legend, the reader is referred to the web version of this article.)

Section 3.3). Increasing IN concentration by 100 times also has little impact on cloud water, rain water, and snow. The only significant difference between the low IN and high IN cases is the graupel number mixing ratio in the convective core regions. The high IN case has a doubled peak graupel number mixing ratio from the low IN case in the mature stage. This is because the enhanced heterogeneous ice nucleation below 9 km in the 100 L^{-1} case (as discussed in Section 3.3) leads to enhanced growth of ice crystals, enhanced formation of graupels, and stronger depletion of cloud droplets. The increase of graupel number mixing ratio by IN is obvious only in the mature stage when the cloud droplet supply is abundant for graupel formation. The number and mass mixing ratios of all hydrometeors in the intermediate case (10 L^{-1}) are also similar to that in the low IN case. The minor difference of the profiles of hydrometeor mass and number mixing ratios between the low, intermediate, and high IN cases also results in the minor difference of rain water approaching the surface. Only in the mature stage, increasing IN concentration slightly increases the rain water mixing ratio by about 20%, while in the developing and dissipating stages, the IN effect on rain water mixing ratio is insignificant.

Fig. 6 shows the vertical profiles of the cloud-averaged number and mass mixing ratios of all hydrometeors for the low IN case (1 L^{-1}) and extremely high IN case (1000 L^{-1}). In the 1000 L^{-1} case, ice number mixing ratio in the anvil regions is significantly lower than the low IN case, especially in the developing stage (~ 62% near the peak). This is because in the developing stage, increasing IN concentration by 1000 times significantly suppresses the homogeneous freezing of cloud droplets and slightly suppresses the homogenous freezing of haze particles, and hence decreases the overall ice formation rate for the layer of 9–14 km, where most of the ice crystals are produced (see Section 3.3). The IN effect on the microphysical properties in the convective core regions below the cloud anvil is also noticeable. Both snow and graupel mainly form and exist in the convective core regions below 9 km. The overall ice formation rate below 9 km is significantly higher as IN concentration is increased by 1000 times, because the heterogeneous ice nucleation processes are enhanced (see Section 3.3). This leads to more ice particles available for conversion into snow particles (including aggregation of ice crystals and collection of ice crystals by snow particles), and hence significantly increases the snow number mixing ratios. The peak snow number mixing ratio is increased by four times in the developing stage and two times in the mature and dissipating stages. Correspondingly, snow mass mixing ratio also increased by near 50% in the mature stage. The graupel number mixing ratio in the mature stage is slightly increased by up to 20% as IN concentration is increased by 1000 times. That is because more ice crystals and snow particles produced below 9 km in the extremely high IN case enhance the riming process. The increase of graupel number mixing ratio with an increase of IN concentration by 1000 times is much less obvious than that with an increase of IN concentration by 100 times. That is because the significantly enhanced heterogeneous nucleation converts more liquid water in the mixed-phase layer into ice crystals, and the enhanced

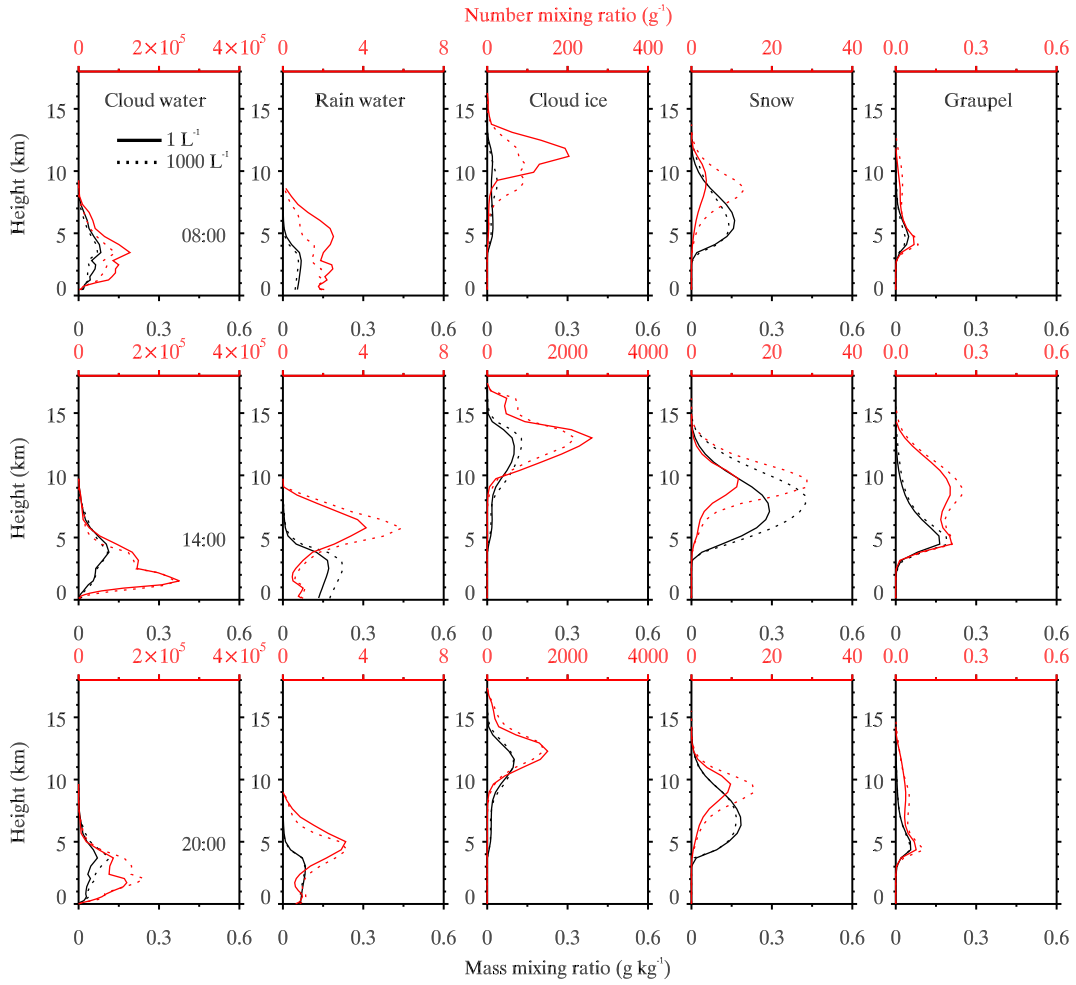

Fig. 6. The same as Fig. 5, but the solid lines and dotted lines are for the low IN case (1 L^{-1}) and extremely high IN case (1000 L^{-1}) respectively.

riming process is restricted by the limitation of liquid water content. The snow and graupel particles can fall down and melt into raindrops below the 0 °C level. The increased snow and graupel in the high IN case hence leads to 30% more rain water mass mixing ratio approaching the surface in the mature stage.

3.5. The IN effect on the surface precipitation and updraft velocity of the deep convective cloud

Fig. 7a–d show the simulated 24-h accumulated surface precipitation from local time 2:00 on 17 April to 2:00 on 18 April under different IN concentration. The observed 24-h accumulated surface precipitation at the surface stations operated by CMA (Chinese Meteorological Society) is also shown as the color dots in Fig. 7a–d, with a maximum of 72.9 mm. The general characteristics of the simulated 24-h accumulated surface precipitation, including the magnitude and spatial distribution of the precipitation, and the approximate moving track of the deep convective cloud, are very similar in different cases. The simulated 24-h accumulated precipitation in all cases is all similar to the observation at the surface stations.

The temporal evolutions of the cloud-averaged surface precipitation and the cloud-averaged updraft velocity in all cases are shown in the Fig. 7e and f. In all cases, the cloud-averaged surface precipitation and the cloud-averaged updraft velocity both evolve similarly with time. From 6:00 to 10:00, when the deep convective cloud is in the developing sage, surface precipitation and updraft velocity are relatively small, and change very slightly with time. From 10:00 to 14:00, as the deep convective cloud reaches the mature stage, surface precipitation and updraft velocity both increase rapidly. From 15:00 to 18:00, the deep convective cloud is still in the mature stage but gradually weakens, as a result, both surface precipitation and updraft velocity decrease. After 18:00, as the convective cloud evolves into the dissipating stage, surface precipitation and updraft velocity become relatively small again.

Surface precipitation in the cases with IN concentration of 10, 100, and 1000 L^{-1} are generally similar to those in the low IN case (1 L^{-1}). Increasing IN concentration may slightly increases the cloud-averaged surface precipitation. The increase is only about 8% averaged throughout the evolution of the deep convective cloud (from 6:00 to 22:00) for an increases of 100 times in IN concentration, and is even less for an increase of 10 or 1000 times in IN concentration. In addition, the increase of surface precipitation with the increased IN concentration is only significant from 14:00–16:00, when the deep convective cloud is relatively mature, with the increase of surface precipitation up to about 21% in the high IN case and 25% in the extremely high IN case at 15:00. In the mature stage, increasing IN concentration leads to slightly higher rain mixing ratio near the surface (Figs. 5 and 6) and hence a little more precipitation. In the developing and dissipating stages, surface precipitation in all cases is similar, which is consistent with the similar rain water mixing ratio at that time.

The cloud-averaged updraft velocity also increases slightly when IN concentration is increased. The averaged increase of updraft velocity throughout the evolution of the deep convective cloud is only 5% when IN concentration is increased by 100 times, and only 2% when IN concentration is increased by 10 or 1000 times. The IN effect on the temporal evolutions of the maximum updraft velocity is also relatively

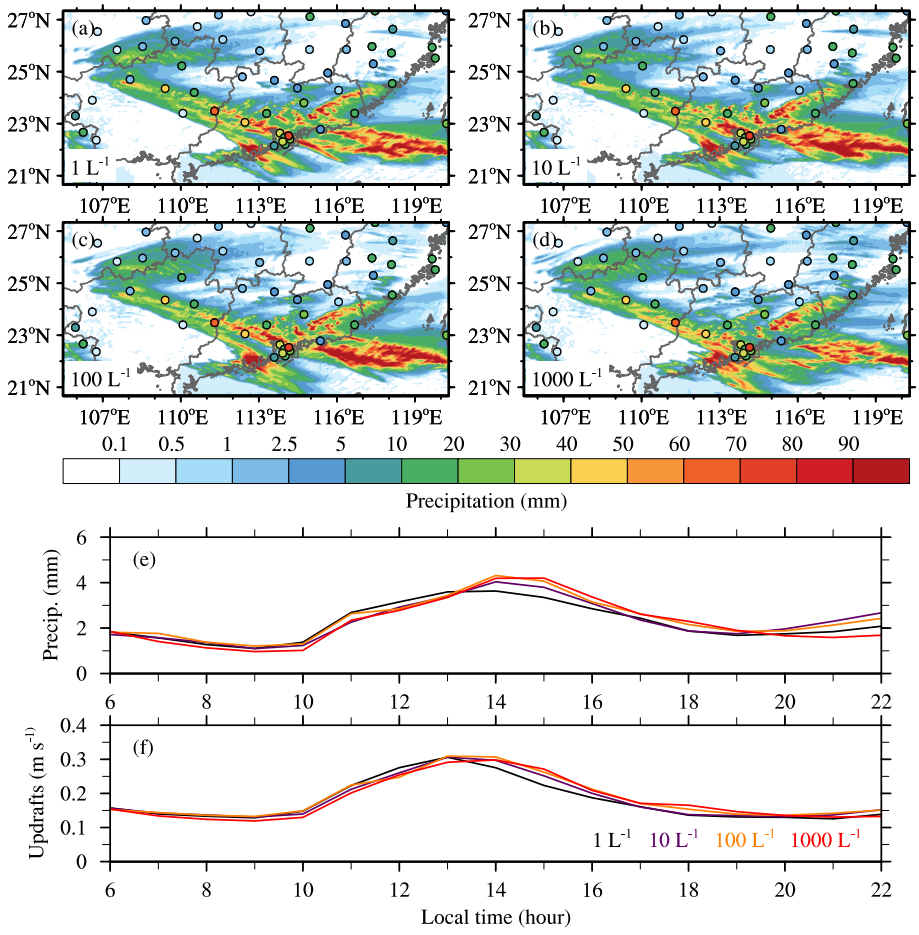

Fig. 7. The simulated 24-h accumulated precipitation during local time 2:00 17 and 2:00 18 April 2011 for the (a) low IN case (1 L^{-1}), (b) intermediate IN case (10 L^{-1}), (c) high IN case (100 L^{-1}), (d) extremely high IN case (1000 L^{-1}). The color dots in (a–d) represent the surface station observed 24-h accumulated precipitation. The temporal evolutions of the cloud-averaged (e) surface precipitation and (f) updraft velocity. The black, purple, orange, and red lines in (e–f) indicate for low, intermediate, high, and extremely high IN cases respectively. (For interpretation of the references to color in this figure legend, the reader is referred to the web version of this article.)

small (figure not shown). The vertical profiles of the cloud-averaged updraft velocity at all stages in the intermediate, high, and extremely high IN cases are all similar to those in the low IN case, as shown with the blue lines in the right column of Fig. 3.

4. Discussions

This study finds that the competition between the heterogeneous nucleation and the homogeneous freezing is really important in determining the cloud microphysical properties, especially in the anvil regions. Our results show that when IN concentration is relatively high, the homogeneous freezing of cloud droplets and haze particles can be weakened or even suppressed. This subsequently leads to the decrease of ice number mixing ratio in the anvil regions (approximately above 9 km). This finding is generally consistent with Phillips et al. (2007), which found the ice concentration can be reduced by up to 1 order of magnitude above 8 km due to the weaker homogeneous freezing of cloud droplets and aerosols. Our results further show that the IN effect on the homogenous freezing of cloud droplets depends on the development stages of the deep convective cloud for the extremely high IN case. The decrease of ice in the anvil regions only occurs in the developing stage, when the updrafts are relatively low. The IN effect depends on the updraft velocity, which is also related to the competition between the heterogeneous and homogeneous nucleation. This agrees well with the parcel model results by Li et al. (2013). They found that when the updrafts are weak, a relatively low IN number concentration is enough for heterogeneous nucleation to dominate over homogeneous nucleation, and when the updrafts are strong, an unrealistically high IN concentration is required for heterogeneous nucleation to dominate the ice formation.

This study also finds that increasing IN concentration can increase the amount of ice particles (including ice, snow, and graupel), which is consistent with the previous studies (e.g., van den Heever et al., 2006; Carrió et al., 2007; Fan et al., 2010). We further show that this effect is mainly revealed in the convective core regions below the cloud anvil (approximately below 9 km), and the IN effect is more obvious on the number mixing ratio than on the mass mixing ratio of ice particles. The different IN effect on anvil and convective core regions indicates that we need to discuss the IN effect on the anvil regions and convective core regions of the deep convective clouds separately.

The sensitivity of the microphysical properties, precipitation, updraft velocity to IN concentration may vary widely in different studies. The chosen cases, as well as the models, especial ice nucleation parameterization in the model, may both affect the IN effect on deep convective clouds, leading to large uncertainty of the IN effect. Different cases may have different cloud base temperature, different humidity, different mixed-phase layer thickness, as well as different liquid water content and ice water content. Then the cloud microphysical processes and their sensitivity to IN concentration may be quite different. For example, Fan et al. (2010) showed that the IN effect on microphysical properties such as ice number concentration and ice water content is very obvious under the more humid condition, while nearly unnoticeable under the less humid condition. The parameterizations in models, especially the ice nucleation parameterization, as well as the setup of aerosol field (including the concentrations and profiles) may vary between various studies, which may also affect the IN effect on deep convective cloud significantly. Our current knowledge about ice nucleation is still insufficient, and the parameterization of ice nucleation and the quantification of IN effect on clouds in models are still difficult (Tao et al., 2012). We hence should better parameterize the

heterogeneous and homogeneous nucleation process and the competition between them in the model.

One of the possible improvements of the ice nucleation parameterization is to take the spatial and temporal variability IN concentration into consideration. In most of the previous studies, ice formation rate is calculated with a constant IN concentration over the simulation domain and time (e.g., the original NSSL scheme), or even without any consideration of IN concentration at all (e.g., Meyers et al., 1992). This is in contrary to the large spatiotemporal variability of IN aerosols. It is found that deep convective clouds play an essential role in the vertical transport of aerosols, which agrees well with previous studies (e.g., Yin et al., 2005; Fu et al., 2017) and can result in large spatiotemporal variability of IN aerosols. Another possible improvement of the ice nucleation parameterization is to include all ice nucleation modes, or at least to include the dominant ice nucleation mode. The dominant ice nucleation mode depends on the occurrence conditions, and hence the heights of the deep convective clouds or even the cloud types. The essential ice nucleation modes consequently may be different in different heights or cases.

One of the most significant IN effects on the microphysical properties in this study is the decreased ice number concentration in the anvil regions. This may significantly change the radiative properties of the anvil of the deep convective cloud. Previous studies have also pointed out that IN aerosols can significantly change the microphysical properties in cloud anvils of the deep convective clouds, especially the ice mass and number concentrations (e.g., Fan et al., 2010). The change of microphysical properties due to aerosols can significantly affect the radiation budget. For example, the larger amount of smaller and longer-lasting ice particles in anvil regions due to the aerosol indirect effect can drive an atmospheric radiative warming of 3–5 $W\,m^{-2}$ and a surface cooling of 5–8 $W\,m^{-2}$ (Fan et al., 2013).

5. Conclusion

This study uses the WRF model to investigate the effect of IN aerosols on a deep convective cloud in South China, as well as the vertical transport of IN aerosols by the deep convective cloud. Four cases with initial surface IN aerosol concentrations of 1, 10, 100, and 1000 L^{-1} are simulated. All the simulations well reproduce the observed evolution of the deep convective cloud and the spatial distribution of precipitation. The deep convective cloud can efficiently transport IN aerosols upwards to altitudes with temperature colder than 0 °C, leading to a large variability of the IN aerosol concentration in time and space.

In the low IN case (1 L^{-1}), it is found that different ice nucleation mode prefers to occur at different temperature range, and hence dominates at different height. Ice nucleation below 7 km is dominated by contact freezing, while for the layers of 7–9 km and above 14 km, ice nucleation is dominated by deposition-nucleation/condensation-freezing. Homogenous freezing of cloud droplets dominates ice formation in the layer of 9–11 km, although immersion freezing, deposition-nucleation/condensation-freezing, and contact freezing also occur in this layer. For the layer of 11–14 km, ice formation is dominated by the homogenous freezing of haze particles.

When IN concentration is higher (10 and 100 L^{-1}), the dominant nucleation mode in each layer remains the same as that in the low IN case. All heterogeneous nucleation modes are significantly enhanced, but homogenous freezing of cloud droplets and haze particles still dominate ice nucleation in the layer of 9–11 km and 11–14 km, where most of the ice crystals are produced. Microphysical properties, surface precipitation and updraft velocity of the deep convective cloud are generally similar to the low IN case.

When IN concentration is increased to be extremely high (1000 L^{-1}), the dominant ice nucleation not only depends on the height, but also depends on the amount of liquid water and hence the development stages of the deep convective cloud. All heterogeneous nucleation modes are further enhanced in this case. The significantly enhanced heterogeneous nucleation could be comparable with or even suppress the homogenous freezing of cloud droplets, and hence leads to significant changes in the microphysical properties. The overall ice formation rate from 9 to 14 km in the extremely high IN case (1000 L^{-1}) is significantly lower than that in the low IN case (1 L^{-1}), especially in the developing stage. In the anvil regions, ice number mixing ratio is consequently lower when the IN concentration is increased by 1000 times. In the convective core regions below the cloud anvil (approximately below 9 km), the enhanced heterogeneous nucleation produces more ice crystals. This increases the amount of ice that are available for the conversion to snow particles, leading to an increase of snow number mixing ratio by more than twice. However, the IN effect on the spatial distribution of precipitation, as well as the temporal evolutions of the cloud-averaged precipitation and updraft velocity is still very small.

Acknowledgements

This study is supported by Chinese NSF grant 41330421 and 973 project 2013CB955803. Discussions with Jost Heintzenberg are greatly appreciated.

References

Bigg, E.K., 1953. The formation of atmospheric ice crystals by the freezing of droplets. Quart. J. Roy. Meteor. Soc. 79, 510–519. http://dx.doi.org/10.1002/qj.49707934207.

Carrió, G.G., van den Heever, S.C., Cotton, W.R., 2007. Impacts of nucleating aerosol on anvil-cirrus clouds: a modeling study. Atmos. Res. 84, 111–131. http://dx.doi.org/10.1016/j.atmosres.2006.06.002.

Chen, F., Dudhia, J., 2001. Coupling an advanced land surface–hydrology model with the Penn State–NCAR MM5 modeling system. Part I: Model implementation and sensitivity. Mon. Weather Rev. 129, 569–585. http://dx.doi.org/10.1175/1520-0493(2001)129<0569:CAALSH>2.0.CO;2.

Chou, M., Suarez, M., 1999. A solar radiation parameterization (CLIRAD-SW) for atmospheric studies. NASA Tech. Memo. 104606, 40.

Connolly, P.J., Choularton, T.W., Gallagher, M.W., Bower, K.N., Flynn, M.J., Whiteway, J.A., 2006. Cloud-resolving simulations of intense tropical Hector thunderstorms: implications for aerosol–cloud interactions. Quart. J. Roy. Meteor. Soc. 132, 3079–3106. http://dx.doi.org/10.1256/qj.05.86.

Cotton, W.R., Tripoli, G.J., Rauber, R.M., Mulvihill, E.A., 1986. Numerical simulation of the effects of varying ice crystal nucleation rates and aggregation processes on orographic snowfall. J. Clim. Appl. Meteorol. 25, 1658–1680. http://dx.doi.org/10.1175/1520-0450(1986)025<1658:NSOTEO>2.0.CO;2.

DeMott, P.J., 1990. An exploratory study of ice nucleation by soot aerosols. J. Appl. Meteorol. 29, 1072–1079. http://dx.doi.org/10.1175/1520-0450(1990)029<1072:AESOIN>2.0.CO;2.

DeMott, P.J., Meyers, M.P., Cotton, W.R., 1994. Parameterization and impact of ice initiation processes relevant to numerical model simulations of cirrus clouds. J. Atmos. Sci. 51, 77–90. http://dx.doi.org/10.1175/1520-0469(1994)051<0077:PAIOII>2.0.CO;2.

DeMott, P.J., Cziczo, D.J., Prenni, A.J., Murphy, D.M., Kreidenweis, S.M., Thomson, D.S., Borys, R., Rogers, D.C., 2003a. Measurements of the concentration and composition of nuclei for cirrus formation. Proc. Natl. Acad. Sci. 100, 14655–14660. http://dx.doi.org/10.1073/pnas.2532677100.

DeMott, P.J., Sassen, K., Poellot, M.R., Baumgardner, D., Rogers, D.C., Brooks, S.D., Prenni, A.J., Kreidenweis, S.M., 2003b. African dust aerosols as atmospheric ice nuclei. Geophys. Res. Lett. 30. http://dx.doi.org/10.1029/2003gl017410.

Deng, Z.Z., Zhao, C.S., Ma, N., Ran, L., Zhou, G.Q., Lu, D.R., Zhou, X.J., 2013. An examination of parameterizations for the CCN number concentration based on in situ measurements of aerosol activation properties in the North China plain. Atmos. Chem. Phys. 13, 6227–6237. http://dx.doi.org/10.5194/acp-13-6227-2013.

Ekman, A.M.L., Engström, A., Wang, C., 2007. The effect of aerosol composition and concentration on the development and anvil properties of a continental deep convective cloud. Quart. J. Roy. Meteor. Soc. 133, 1439–1452. http://dx.doi.org/10.1002/qj.108.

Fan, J., Comstock, J.M., Ovchinnikov, M., 2010. The cloud condensation nuclei and ice nuclei effects on tropical anvil characteristics and water vapor of the tropical tropopause layer. Environ. Res. Lett. 5, 044005. http://dx.doi.org/10.1088/1748-9326/5/4/044005.

Fan, J., Leung, L.R., Rosenfeld, D., Chen, Q., Li, Z., Zhang, J., Yan, H., 2013. Microphysical effects determine macrophysical response for aerosol impacts on deep convective clouds. Proc. Natl. Acad. Sci. 110, E4581–E4590. http://dx.doi.org/10.1073/pnas.1316830110.

Fornea, A.P., Brooks, S.D., Dooley, J.B., Saha, A., 2009. Heterogeneous freezing of ice on atmospheric aerosols containing ash, soot, and soil. J. Geophys. Res. 114. http://dx.doi.org/10.1029/2009jd011958.

Fu, S., Deng, X., Li, Z., Xue, H., 2017. Radiative effect of black carbon aerosol on a squall line case in North China. Atmos. Res. 197, 407–414. http://dx.doi.org/10.1016/j.atmosres.2017.07.026.

Grell, G.A., Freitas, S.R., 2013. A scale and aerosol aware stochastic convective parameterization for weather and air quality modeling. Atmos. Chem. Phys. 13, 23845–23893. http://dx.doi.org/10.5194/acpd-13-23845-2013.

Hallett, J., Mossop, S.C., 1974. Production of secondary ice particles during the riming process. Nature 249, 26. http://dx.doi.org/10.1038/249026a0.

Hazra, A., Padmakumari, B., Maheskumar, R.S., Chen, J.-P., 2016. The effect of mineral dust and soot aerosols on ice microphysics near the foothills of the Himalayas: a numerical investigation. Atmos. Res. 171, 41–55. http://dx.doi.org/10.1016/j.atmosres.2015.12.005.

van den Heever, S.C., Carrió, G.G., Cotton, W.R., DeMott, P.J., Prenni, A.J., 2006. Impacts of nucleating aerosol on Florida storms. Part I: Mesoscale simulations. J. Atmos. Sci. 63, 1752–1775. http://dx.doi.org/10.1175/JAS3713.1.

Hiron, T., Flossmann, A.I., 2015. A study of the role of the parameterization of heterogeneous ice nucleation for the modeling of microphysics and precipitation of a convective cloud. J. Atmos. Sci. 72, 3322–3339. http://dx.doi.org/10.1175/jas-d-15-0026.1.

Hong, S.-Y., Noh, Y., Dudhia, J., 2006. A new vertical diffusion package with an explicit treatment of entrainment processes. Mon. Weather Rev. 134, 2318–2341. http://dx.doi.org/10.1175/MWR3199.1.

Hoose, C., Möhler, O., 2012. Heterogeneous ice nucleation on atmospheric aerosols: a review of results from laboratory experiments. Atmos. Chem. Phys. 12, 9817–9854. http://dx.doi.org/10.5194/acp-12-9817-2012.

Jiang, H., Yin, Y., Yang, L., Yang, S., Su, H., Chen, K., 2014. The characteristics of atmospheric ice nuclei measured at different altitudes in the Huangshan Mountains in Southeast China. Adv. Atmos. Sci. 31, 396–406. http://dx.doi.org/10.1007/s00376-013-3048-5.

Jiang, H., Yin, Y., Wang, X., Gao, R., Yuan, L., Chen, K., Shan, Y., 2016. The measurement and parameterization of ice nucleating particles in different backgrounds of China. Atmos. Res. 181, 72–80. http://dx.doi.org/10.1016/j.atmosres.2016.06.013.

Lamb, D., Verlinde, J., 2011. Physics and Chemistry of Clouds. Cambridge University Press, Cambridge, pp. 584.

Léon, J.-F., Derimian, Y., Chiapello, I., Tanr'e, D., Podvin, T., Chatenet, B., Diallo, A., Deroo, C., 2009. Aerosol vertical distribution and optical properties over M'Bour (16.96° W; 14.39° N), Senegal from 2006 to 2008. Atmos. Chem. Phys. 9, 9249–9261. http://dx.doi.org/10.5194/acp-9-9249-2009.

Li, Z., Xue, H., Yang, F., 2013. A modeling study of ice formation affected by aerosols. J. Geophys. Res. 118, 11,213–211,227. http://dx.doi.org/10.1002/jgrd.50861.

Mansell, E.R., Ziegler, C.L., Bruning, E.C., 2010. Simulated electrification of a small thunderstorm with two-moment bulk microphysics. J. Atmos. Sci. 67, 171–194. http://dx.doi.org/10.1175/2009jas2965.1.

Meyers, M.P., DeMott, P.J., Cotton, W.R., 1992. New primary ice-nucleation parameterizations in an explicit cloud model. J. Appl. Meteorol. 31, 708–721. http://dx.doi.org/10.1175/1520-0450(1992)031<0708:NPINPI>2.0.CO;2.

Mlawer, E.J., Taubman, S.J., Brown, P.D., Iacono, M.J., Clough, S.A., 1997. Radiative transfer for inhomogeneous atmospheres: RRTM, a validated correlated-k model for the longwave. J. Geophys. Res. 102, 16663–16682. http://dx.doi.org/10.1029/97jd00237.

Mossop, S.C., 1970. Concentrations of ice crystals in clouds. Bull. Am. Meteorol. Soc. 51, 474–479. http://dx.doi.org/10.1175/1520-0477(1970)051<0474:COICIC>2.0.CO;2.

Mossop, S.C., Hallett, J., 1974. Ice crystal concentration in cumulus clouds: influence of the drop spectrum. Science 186, 632–634. http://dx.doi.org/10.1126/science.186.4164.632.

Murray, B.J., Broadley, S.L., Wilson, T.W., Atkinson, J.D., Wills, R.H., 2011. Heterogeneous freezing of water droplets containing kaolinite particles. Atmos. Chem. Phys. 11, 4191–4207. http://dx.doi.org/10.5194/acp-11-4191-2011.

Murray, B.J., O'Sullivan, D., Atkinson, J.D., Webb, M.E., 2012. Ice nucleation by particles immersed in supercooled cloud droplets. Chem. Soc. Rev. 41, 6519–6554. http://dx.doi.org/10.1039/c2cs35200a.

Phillips, V.T.J., Donner, L.J., Garner, S.T., 2007. Nucleation processes in deep convection simulated by a cloud-system-resolving model with double-moment bulk microphysics. J. Atmos. Sci. 64, 738–761. http://dx.doi.org/10.1175/jas3869.1.

Pruppacher, H.R., Klett, J.D., 1997. Microphysics of Clouds and Precipitation. Kluwer Academic Publishers, Dordrecht, pp. 954.

Rogers, D.C., DeMott, P.J., Kreidenweis, S.M., Chen, Y., 1998. Measurements of ice nucleating aerosols during SUCCESS. Geophys. Res. Lett. 25, 1383–1386. http://dx.doi.org/10.1029/97gl03478.

Rose, D., Nowak, A., Achtert, P., Wiedensohler, A., Hu, M., Shao, M., Zhang, Y., Andreae, M.O., Pöschl, U., 2010. Cloud condensation nuclei in polluted air and biomass burning smoke near the mega-city Guangzhou, China–part 1: size-resolved measurements and implications for the modeling of aerosol particle hygroscopicity and CCN activity. Atmos. Chem. Phys. 10, 3365–3383.

Schuur, T.J., Rutledge, S.A., 2000. Electrification of Stratiform regions in mesoscale convective systems. Part II: two-dimensional numerical model simulations of a symmetric MCS. J. Atmos. Sci. 57, 1983–2006. http://dx.doi.org/10.1175/1520-0469(2000)057<1983:EOSRIM>2.0.CO;2.

Tao, W.K., Chen, J.P., Li, Z., Wang, C., Zhang, C., 2012. Impact of aerosols on convective clouds and precipitation. Rev. Geophys. 50, RG2001. http://dx.doi.org/10.1029/2011RG000369.

Twohy, C.H., 2015. Measurements of Saharan dust in convective clouds over the tropical eastern Atlantic Ocean. J. Atmos. Sci. 72, 75–81. http://dx.doi.org/10.1175/jas-d-14-0133.1.

Twohy, C., Poellot, M., 2005. Chemical characteristics of ice residual nuclei in anvil cirrus clouds: evidence for homogeneous and heterogeneous ice formation. Atmos. Chem. Phys. 5, 2289–2297. http://dx.doi.org/10.5194/acp-5-2289-2005.

Twomey, S., 1959. The nuclei of natural cloud formation part II: the supersaturation in natural clouds and the variation of cloud droplet concentration. Pure Appl. Geophys. 43, 243–249.

Walko, R.L., Cotton, W.R., Meyers, M., Harrington, J., 1995. New RAMS cloud microphysics parameterization part I: the single-moment scheme. Atmos. Res. 38, 29–62. http://dx.doi.org/10.1016/0169-8095(94)00087-T.

Wang, B., Lambe, A.T., Massoli, P., Onasch, T.B., Davidovits, P., Worsnop, D.R., Knopf, D.A., 2012. The deposition ice nucleation and immersion freezing potential of amorphous secondary organic aerosol: Pathways for ice and mixed-phase cloud formation. J. Geophys. Res. 117http://dx.doi.org/10.1029/2012jd018063. (n/a-n/a).

Yin, Y., Carslaw, K.S., Feingold, G., 2005. Vertical transport and processing of aerosols in a mixed-phase convective cloud and the feedback on cloud development. Quart. J. Roy. Meteorol. Soc. 131, 221–245. http://dx.doi.org/10.1256/qj.03.186.

Yin, J., Wang, D., Zhai, G., 2012. An evaluation of ice nuclei characteristics from the long-term measurement data over North China. Asia-Pac. J. Atmos. Sci. 48, 197–204. http://dx.doi.org/10.1007/s13143-012-0020-8.

Yu, H., Chin, M., Winker, D.M., Omar, A.H., Liu, Z., Kittaka, C., Diehl, T., 2010. Global view of aerosol vertical distributions from CALIPSO lidar measurements and GOCART simulations: regional and seasonal variations. J. Geophys. Res. 115. http://dx.doi.org/10.1029/2009jd013364.

Ziegler, C.L., Ray, P.S., MacGorman, D.R., 1986. Relations of kinematics, microphysics and electrification in an isolated mountain thunderstorm. J. Atmos. Sci. 43, 2098–2115. http://dx.doi.org/10.1175/1520-0469(1986)043<2098:ROKMAE>2.0.CO;2.